ACS APPLIED MATERIALS & INTERFACES

Research Article

www.acsami.org

Graphene Quantum Dot Layers with Energy-Down-Shift Effect on Crystalline-Silicon Solar Cells

Kyung D. Lee,[†] Myung J. Park,[‡] Do-Yeon Kim,[§] Soo M. Kim,[†] Byungjun Kang,[†] Seongtak Kim,[†] Hyunho Kim,[†] Hae-Seok Lee,*[,†] Yoonmook Kang,*[,∥] Sam S. Yoon,[§] Byung H. Hong,[‡] and Donghwan Kim*[,†]

[†]Department of Materials Science and Engineering, Solar Energy Research Center of Korea University, 145 Anam-ro, Seongbuk-gu, Seoul 136-713, Korea

[‡]Department of Chemistry, College of Natural Sciences, Seoul National University, Daehack-dong, Gwanak-gu, Seoul 151-747, Korea

[§]Department of Mechanical Engineering, Korea University, 145 Anam-ro, Seongbuk-gu, Seoul 136-713, Korea

[∥]KU-KIST Green School - Graduate School of Energy and Environment, Korea University, 145 Anam-ro, Seongbuk-gu, Seoul 136-713, Korea

Supporting Information

ABSTRACT: Graphene quantum dot (GQD) layers were deposited as an energy-down-shift layer on crystalline-silicon solar cell surfaces by kinetic spraying of GQD suspensions. A supersonic air jet was used to accelerate the GQDs onto the surfaces. Here, we report the coating results on a silicon substrate and the GQDs' application as an energy-down-shift layer in crystalline-silicon solar cells, which enhanced the power conversion efficiency (PCE). GQD layers deposited at nozzle scan speeds of 40, 30, 20, and 10 mm/s were evaluated after they were used to fabricate crystalline-silicon solar cells; the results indicate that GQDs play an important role in increasing the optical absorptivity of the cells. The short-circuit current density was enhanced by about 2.94% (0.9 mA/cm^2) at 30 mm/s. Compared to a reference device without a GQD energy-down-shift layer, the PCE of p-type silicon solar cells was improved by 2.7% (0.4 percentage points).

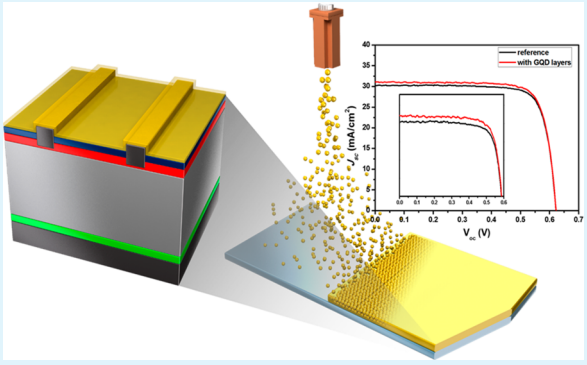

KEYWORDS: *graphene quantum dots, silicon solar cells, GQD layers, energy-down-shift, light absorption*

INTRODUCTION

Conventional silicon solar cells effectively convert only photons with energy close to the silicon bandgap as a result of the mismatch between the incident solar spectrum and the spectral absorption properties of the material. Photons with energy (E_{ph}) smaller than the bandgap are not absorbed. If E_{ph} is larger than the bandgap (E_g), the photons are absorbed, but the excess energy ($E_{ph} - E_g$) is not used effectively owing to electron thermalization. The response of silicon solar cells in the UV region is poorer than that in the visible range. In the last few decades, much research has been conducted to improve the power conversion efficiency (PCE, or η) of silicon solar cells by surface texturing,[1−3] adding an antireflection coating,[4,5] changing the doping concentration,[6,7] metallization,[8−10] and designing new structures using n-type silicon wafers.[11−15] Nanopatterned structures and metal nanoparticles were recently used to exploit the plasmon effects of light scattering onto the solar-cell surface to improve the light absorption in the UV region and the photocurrent.[16−18] However, there are many challenges and limitations owing to the fast decaying nature of the plasmon effects of controlled metal nanoparticles on silicon solar cells, and it is difficult to penetrate the SiN_x:H antireflection coating (ARC) for near-field enhancement.[19] Recently, researchers have reported effective use of the plasmon effect for optically thin thin-film solar cells.[20−23] However, the use of newly designed materials including graphene quantum dots (GQDs) as an energy-down-shift layer has not been reported. GQDs are much smaller than graphene sheets and graphene oxide (GO), and they consist of hybrid structures of unique sp2 and sp3 composites.[24,25] GQDs are, therefore, zero-dimensional materials that have size-tunable bandgaps. Bulk graphene has a bandgap of zero; however, size-controlled benzenes, which are composed of graphene components, have bandgaps of zero to a few electronvolts.[26−28] GQDs made of chemically modified graphene exhibit a variety of functional stabilities and also have low toxicity, high fluorescent activity, robust chemical inertness, and excellent water solubility. Therefore, GQDs are potential candidates for use in nano-devices and are suitable for use in optoelectronic devices,[29,30] biological sensing, imaging, organic photovoltaics, and poly-

Received: May 4, 2015
Accepted: August 12, 2015
Published: August 12, 2015

DOI: 10.1021/acsami.5b03672
ACS Appl. Mater. Interfaces 2015, 7, 19043−19049

meric devices.[31,32] On the other hand, these materials are hard to synthesize, and it is difficult to obtain a uniformly thin layer of such material on solid substrates like silicon. For example, producing thin layers of aqueous GQDs for organic photovoltaic or polymeric devices, is especially problematic because GQDs are prone to agglomeration after drying. To overcome this drawback, we used the method of kinetic spray coating, which enables the formation of thin, uniform layers and, as a result, is probably the best among the available methods.[33]

EXPERIMENTAL SECTION

Synthesis of Graphene Quantum Dots. GO was synthesized using the modified Hummer's method.[34] The purified GO was thermally reduced (250 °C, 2 h) inside a box furnace to obtain a fine, uniformly sized (GO) powder.[35] Reduced GO powder (0.5 g) was then added to a mixture of sulfuric and nitric acid and mildly ultrasonically vibrated for 24 h. The acidic ingredients were removed from the solution by diluting the sample with distilled water after centrifuging for 30 min at 4000 rpm. This rinsing process was repeated six times. The sample was subsequently filtrated through a 0.025 μm nanoporous Anodisc, and the resulting filtrate was purified overnight using a 2000 Da dialysis bag. Next, a 3% suspension was synthesized as an aqueous solution for coating the GQD layers.

GQD Layer Coating by Kinetic Spraying Method. The GQD suspension was injected into the kinetic spray equipment, which was designed in-house (Figure S1). The in-house fabricated components included the gas tank, syringe pump, stainless steel nozzle, ultrasonic atomizer, and $x-y$ stage. The optimum settings for GQD coating for the nozzle temperature, syringe pump flow rate, and traversed substrate length per nozzle scan speed were 220 °C, 1 mL/s, and 12 mm/s, respectively (Figures S5 and S7).[33]

The moving nozzle was withdrawn after the solvent evaporates to promote concentration[36] and accumulation[37] of the GQD droplets on the substrate (Figure S1).[33]

Fabrication of Silicon Solar Cells. Pseudosquare crystalline-silicon wafers with a length of 156 mm (6 in.) (area: 156 × 156 mm^2) were used as the starting material. Saw damage marks on the wafers were removed by alkali (KOH) etching at 80 °C for 10 min. Next, using $POCl_3$ as the doping source, the silicon wafers were doped with phosphorus to maintain the sheet resistance in the range of 55−60 Ω/sq. The phosphorus-doped wafers were then treated to remove the phosphorus silica glass (PSG) layer, and the back side of the phosphorus-doped layer was removed by a buffer oxide etchant. A 90 nm-thick SiN_x:H film was then deposited on the front side surface for passivation and antireflection by a plasma-enhanced chemical vapor deposition system (13.56 MHz, Tesolar, TES. Co. Ltd., South Korea).[38] For the metal electrodes of the solar cells, Al paste and Ag paste were screen printed on the back and front sides, respectively. Finally, the printed wafers were cofired using a belt furnace system at 870 °C and a belt feed rate of 4445 mm/min (175 in. per minute (ipm)).

The synthesized GQDs were coated on the front surface of the c-Si solar cell by kinetic spraying.

Characterization. The GQD layers were characterized using various microscopic and spectroscopic techniques. For example, surface micrographs and images were obtained using a high-resolution scanning electron microscope (HRSEM; XL30SFEG, Philips Co., The Netherlands), an optical microscope (OM; STM6, Olympus, Japan), and an atomic force microscope (AFM) in noncontact mode (XE-100, Park System, South Korea). The characteristics of the interface between the substrate and the GQD layer were examined using a transmission electron microscope (TEM) (JEM-2100F, JEOL, Japan) and an energy-dispersive spectrometer (EDS; Oxford Istrument, UK). Furthermore, the corresponding UV−vis absorption and reflection spectra were recorded on a UV−vis spectrophotometer (V-670, JASCO, Japan). Since GQDs are fluorescent materials, their fluorescence—characterized by the photoluminescence (PL)—was measured on a monochromator (MonoRa 750i, DongWoo Optron, South Korea) equipped with a 325 nm laser. In addition, the crystal quality and layer uniformity were determined using Raman spectroscopy (LabRam Aramis IR2, Horiba, Japan) with a 532 nm laser. The elemental composition of the samples was also analyzed by X-ray photoelectron spectroscopy (XPS; PHI X-tool, ULVAC Technologies, Inc., Japan) using an Al K_α X-ray source and an operating voltage of 1486.6 eV. The performance of the solar cells was determined using a solar simulator (WXS-155−10, Wacom, Japan) under AM1.5G illumination in accordance with the international standard IEC-60904 (Class: AAA) by a current−voltage sweep. Furthermore, the external quantum efficiency (EQE) was measured by a solar quantum efficiency measurement system (laboratory-scale EQE system, PV Measurements, U.S.A.).

RESULTS AND DISCUSSION

Fluorescent GQDs were synthesized and coated using a unique kinetic spray deposition technique that supersonically accelerated droplets of GQDs onto silicon-solar-cell surfaces as an energy-down-shift layer. Figure 1 schematically depicts the kinetic spray coating method for energy-down-shift GQD layers. Droplets were supersonically accelerated through a converging−diverging de Laval nozzle.[39] The GQD precursor, an aqueous suspension of GQDs, was injected by air drag into the nozzle throat and atomized by an ultrasonic atomizer upon exposure to the high-speed gas stream.[33] Synthesized GQDs were coated under four different thickness conditions: nozzle scan speeds of 40, 30, 20, and 10 mm/s. We did not consider higher nozzle scan speeds because the process window for coating was 10−40 mm/s. We coated additional GQD layers on the silicon-solar-cell surfaces by kinetic spraying. The short-circuit current density (J_{sc}) varied with the thickness of the GQD layer, but the open-circuit voltage (V_{oc}) and fill factor (FF) did not change. The change in J_{sc} caused the PCE to change, indicating that the improved PCE of silicon solar cell devices with a GQD energy-down-shift layer was relevant to the light-absorption ability and charge-carrier transport at different thicknesses.[40] At a nozzle scan speed of 30 mm/s, the PCE increased from 14.88 to 15.27%.

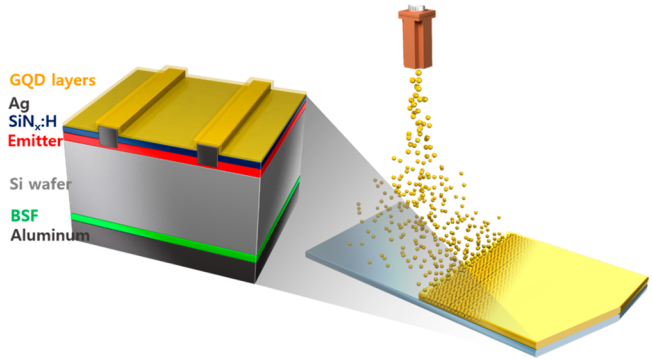

Figure 1. Schematic of a silicon solar cell with energy-down-shift layer of GQDs applied by kinetic spraying.

Figure 2 shows HRSEM and AFM images of the surface microstructure of GQD layers deposited at different nozzle scan speeds. All the scan speeds yielded well-coated GQD layers on hydrophilic silicon nitride surfaces. In particular, the scan speed of 30 mm/s produced the most uniform morphology with small aggregated particles, as shown in Figure 2c,d. In addition, well-defined TEM images of GQD layers on silicon nitride/silicon substrate are shown Figures 3, S2, and S3. In contrast, the layers obtained at 20 and 10 mm/s exhibited strongly

DOI: 10.1021/acsami.5b03672
ACS Appl. Mater. Interfaces 2015, 7, 19043−19049

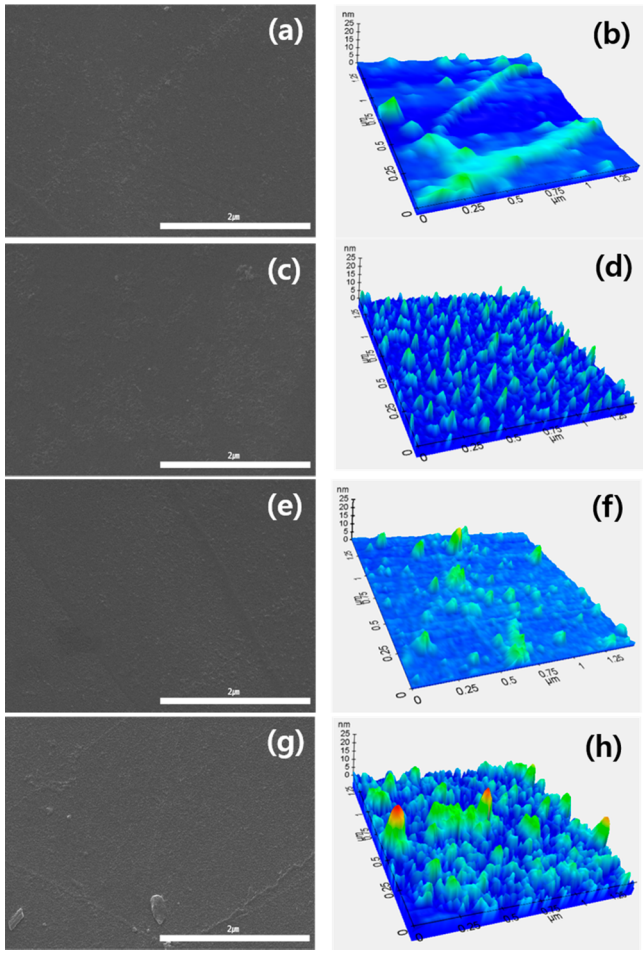

Figure 2. HRSEM and AFM images showing the microstructure of GQD layers deposited by kinetic spraying on a silicon nitride/silicon substrate at nozzle scan speeds of (a and b) 40 mm/s, (c and d) 30 mm/s, (e and f) 20 mm/s, and (g and h) 10 mm/s.

agglomerated and randomly overlapping morphology, as shown in Figure 2e–h.

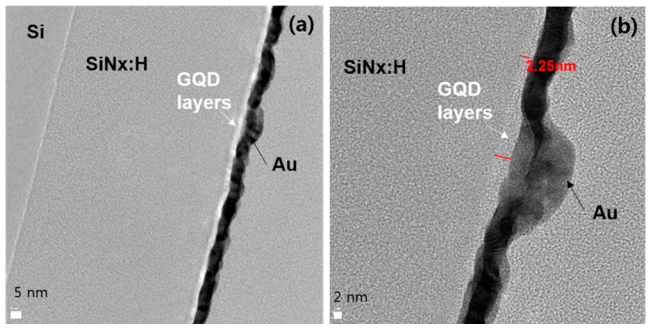

Figure 3. TEM images of GQD layers at 30 mm/s: (a) GQD layers on silicon nitride/silicon and (b) magnified image.

A comparison of the UV–vis absorption spectra of the GQD suspension and coated layers in Figure 4a shows that they exhibited similar absorption peaks at a wavelength of about 375 nm.[41] Compared to the UV–vis spectra, the fluorescence spectra, as characterized by the PL spectra, reveal larger differences between the layers and the suspension. The peak positions of the PL spectra assigned to both samples appear at nearly same position (530 nm). However, the difference of the line width is confirmed in which the deposited GQD layers are deconvolved to five peaks (Figure S4), and it is assumed that line width broadening originates from the annealing process during the coating method. In the kinetic spray process, heat (180 °C) and supersonic kinetic energy were generated on the substrate, which resulted in the reduction of the oxygen functional group coordinated at the edge of GQDs. It could be confirmed by downshift of the G peak position in the Raman spectrum and decreased oxygen peak in the XPS data (Figure 4a,b). Recovery of the aromatic system led to π-stacking of neighboring GQDs, which eventually increased the size effect with red shift of PL peaks.[42,43]

In the drop casting and drying method (Figure S5d–f), the annealing process was also treated and the same PL spectra behavior was conformed. However, the degree of aggregation could not be controlled, which caused the multiple peak with larger red shift. On the other hand, in the spraying method (Figure S5a–c), the peak position and the line width were nearly unchanged, even in adding the number of coating cycle, which means that the spray coating method could give uniformity to any of substrate.

The coated GQD layers and the GQD suspension were also investigated by XPS and Raman spectroscopy. The sp2 carbon peaks in the C 1s photoelectron spectra (Figure 5b) overlap at 284.5 eV. The XPS intensities of carbonyl and carboxyl groups with binding energies of 286–290 eV in the GQD layers, however, were lower than their XPS intensities in the solution. This difference resulted from the substrate temperature during kinetic spray processing and partial chemical doping.[44] Figure 5c,d shows the C 1s photoelectron spectra of the GQD layers and the GQD suspension, respectively. Each C 1s spectrum can be deconvolved into four or five peaks, which correspond to the positions of C=C (284.5 eV), the hydroxyl group (286 eV), C–O (286.5 eV), C=O (288 eV), and HO–C=O (289 ± 0.2 eV). As in the case of the UV–vis spectra (Figure 4a), the XPS results confirmed that the GQD layers and solution shared many similarities. The results of micro-Raman spectroscopy analysis are shown in Figure 5a. Micro-Raman spectroscopy was performed on GQD layers and their aqueous counterparts. Because the aqueous GQDs were drop-casted onto the substrate, they could differ structurally and had different carbon defects compared to the GQD layers. Figure 5a compares the D (~1360 cm^{-1}) and G peaks (~1580 cm^{-1}) of the samples. The G peak represents the hexagonal lattice of graphene, which is associated with the double-degenerate E_{2g} mode, and the D peaks arise because of defects.[45] The D peaks are almost indistinguishable in Figure 5a, and there is only a small difference between the G peaks. The OM images and the areas calculated by a Raman mapping system differed drastically, however, when the layers and the solution were compared (Figure S6).

So far, we have evaluated and confirmed the characteristics of GQD layers obtained by kinetic spraying of a GQD suspension compared with those of the initial synthesized GQD solution. On the basis of the results, we conclude that the GQD layers possessed fluorescence and carbon characteristics similar to those of the solutions. To experimentally verify the positive effects, fluorescent GQD layers were applied to crystalline-silicon solar cells as an energy-down-shift layer at nozzle scan speeds of 40, 30, 20, or 10 mm/s and the cell performance was analyzed.

DOI: 10.1021/acsami.5b03672
ACS Appl. Mater. Interfaces 2015, 7, 19043–19049

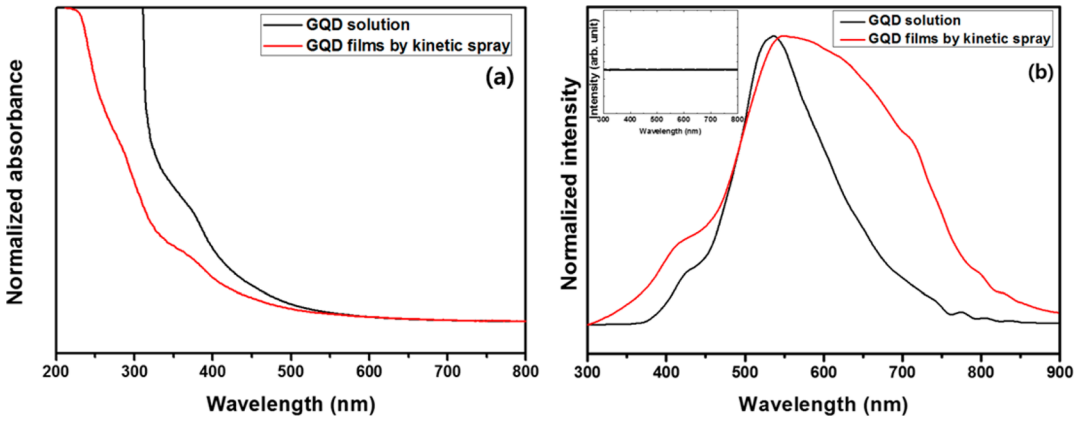

Figure 4. (a) UV−vis absorption spectra and (b) PL spectra of a GQD suspension and GQD layers and (b, inset) PL spectrum of silicon nitride/silicon.

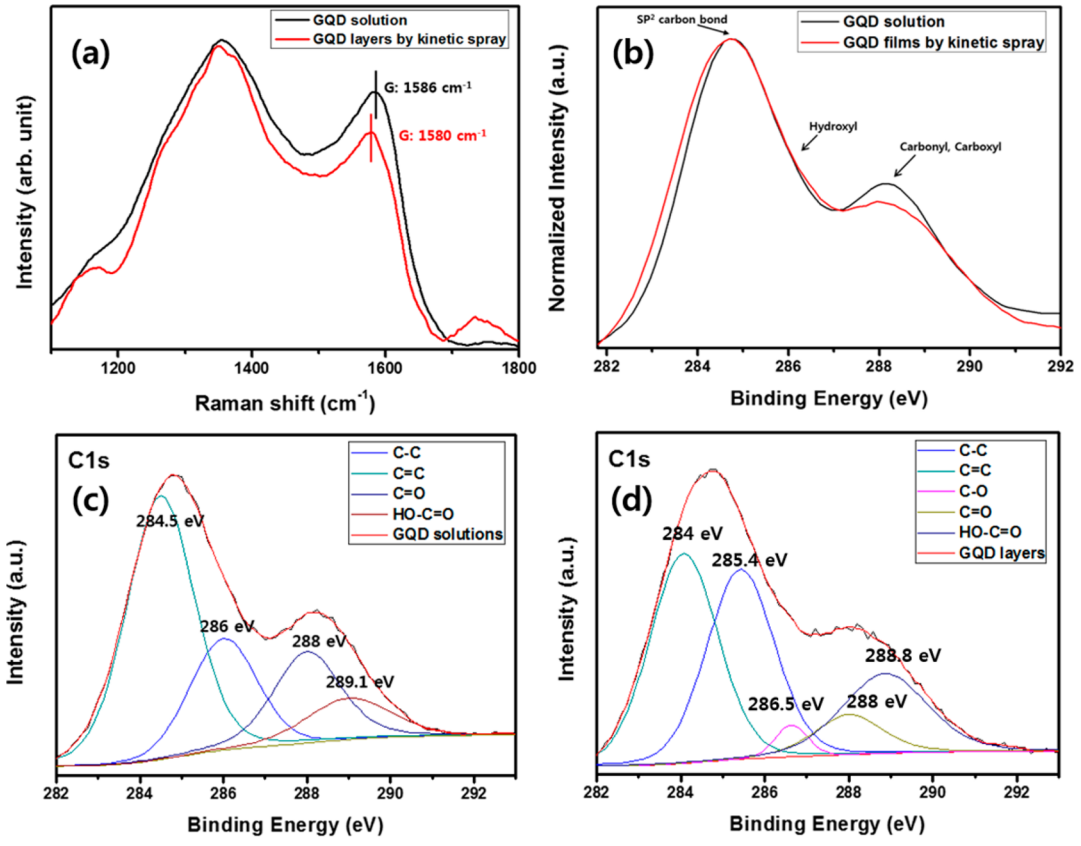

Figure 5. (a) Micro-Raman shift and (b) XPS spectra of the GQD suspension versus GQD layers obtained by kinetic spraying. Deconvolved XPS spectra for the (c) GQD solution and (d) GQD layers.

The structure of the silicon solar cells with energy-down-shift layers is shown in Figure 1. The GQD layers were coated on fabricated silicon solar cells with areas of 4 × 4 cm^2. The down-shift layers were used on a nontextured structure because the surface of a randomly textured pyramid yields diffuse reflections. Therefore, it would have been difficult to conduct an exact analysis of the energy-down-shift effect on the nanoscale. The layers on the solar cells were optimized by using different nozzle scan speeds from 10 to 40 mm/s and a 11 wt % suspension, as shown in Figures S7−9 and Table 1. The parameters of the devices with GQD layers, expressed as the difference between the values with and without the down-shift layer, are shown in Figure 6a,b. In Figure 6a, the highest ΔJ_{sc} value, 0.9 mA/cm^2 (+2.94%), was obtained at a nozzle scan speed of 30 mm/s; this result was related to the highest incident photon to charge carrier efficiency values of the devices with GQD layers. For the cells with GQD layers prepared at 40 and 20 mm/s, J_{sc} improved by 0.2 and 0.4 mA/cm^2, respectively (Table 1). However, a negative value of ΔJ_{sc}, − 0.6 mA/cm^2 (−1.98%), appeared for the cell with GQD layers prepared at 10 mm/s, implying that a high thickness of the GQD layer played a negative role in light absorption. As a result, ΔPCE also showed the same trend for the cells prepared under the four coating conditions. On the other hand, the V_{oc} and FF did not change noticeably in the cells compared to the reference device, as shown in Figure 6b. To understand the

DOI: 10.1021/acsami.5b03672
ACS Appl. Mater. Interfaces 2015, 7, 19043−19049

Table 1. Performance Parameters of Silicon Solar Cells with Energy-Down-Shift Layers of GQDs Deposited at Nozzle Scan Speeds of 40, 30, 20, and 10 mm/s

coating conditions (mm/s)		η (%)	V_{oc} (mV)	J_{sc} (mA/cm^2)	FF (%)	ΔJ_{sc} (mA/cm^2)	change in J_{sc} (%)
40	before	15.23	622	30.69	79.76	+0.2	+0.65
	after	15.29	622	30.89	79.56		
30	before	14.88	622	30.20	79.26	+0.89	+2.94
	after	15.27	622	31.08	79.00		
20	before	15.43	622	30.77	80.56	+0.36	+1.18
	after	15.55	622	31.14	80.28		
10	before	15.21	622	30.65	79.82	−0.61	−1.98
	after	14.93	621	30.04	79.98		

degree to which the energy shift enhanced the photovoltaic performance, we estimated the EQE, as shown in Figures 6c and S8a. In addition, the values of internal quantum efficiency (IQE) of absorbance of the cells, which confirm the energy-shifting effect, are shown in Figures 6d and S8b. All the IQE values of the cells were higher than those of the device without the GQD layer. In particular, the surface exhibited an increased energy-down-shift effect at UV wavelengths (300−420 nm), confirming that the functional group on the edge of the GQD played a positive role in light absorption. For the cell prepared under optimum conditions (deposition at 30 mm/s), the PCE was 15.3% compared to an initial value of 14.9%, which represents ΔPCE of 0.4 percentage points and an improvement in PCE of +2.7%.

CONCLUSION

This study shows that GQD layers can be produced by kinetic spray coating of suspensions onto a silicon substrate. The resulting layers possess fluorescence and carbon characteristics similar to those of the solutions. Finally, we demonstrated that the energy-down-shift performance of silicon solar cells varied with the thickness of GQD layers. The layers absorbed UV light and emit visible light by energy-down-shifting. However, when the GQD layers on the surface were too thick, they played a negative role in silicon solar cells. Consequently, we determined the optimal conditions for coating of GQD layers with maximized light absorptivity on the silicon-solar-cell surface. At a nozzle scan speed of 30 mm/s, the layers shifted the energy from UV wavelengths (300−420 nm) to visible wavelengths (450−750 nm). The greatest increase in J_{sc}, about 0.9 mA/cm^2, was observed at this scan speed. The PCE of the device using the layers deposited at 30 mm/s changed from 14.9 to 15.3%, yielding a + 2.7% increase in efficiency. We conclude that this work confirms that kinetic spray−coating is a viable coating process for nanoelectronics and other silicon-based devices. Kinetic spray coating can, therefore, potentially broaden the range of suitable applications for solution-based materials. Furthermore, this study confirmed the range of light absorptivity for energy-down-shift layers on silicon solar cells that potentially broaden the range of suitable applications for solution-based materials.

ASSOCIATED CONTENT

Supporting Information

The Supporting Information is available free of charge on the ACS Publications website at DOI: 10.1021/acsami.5b03672.

Kinetic spray-coating method, deconvoluted PL spectra of GQD layers, comparison of PL spectra for GQD layers by kinetic spray vs drop-casting operation, TEM images, EDS analysis, Raman mapping, external quantum

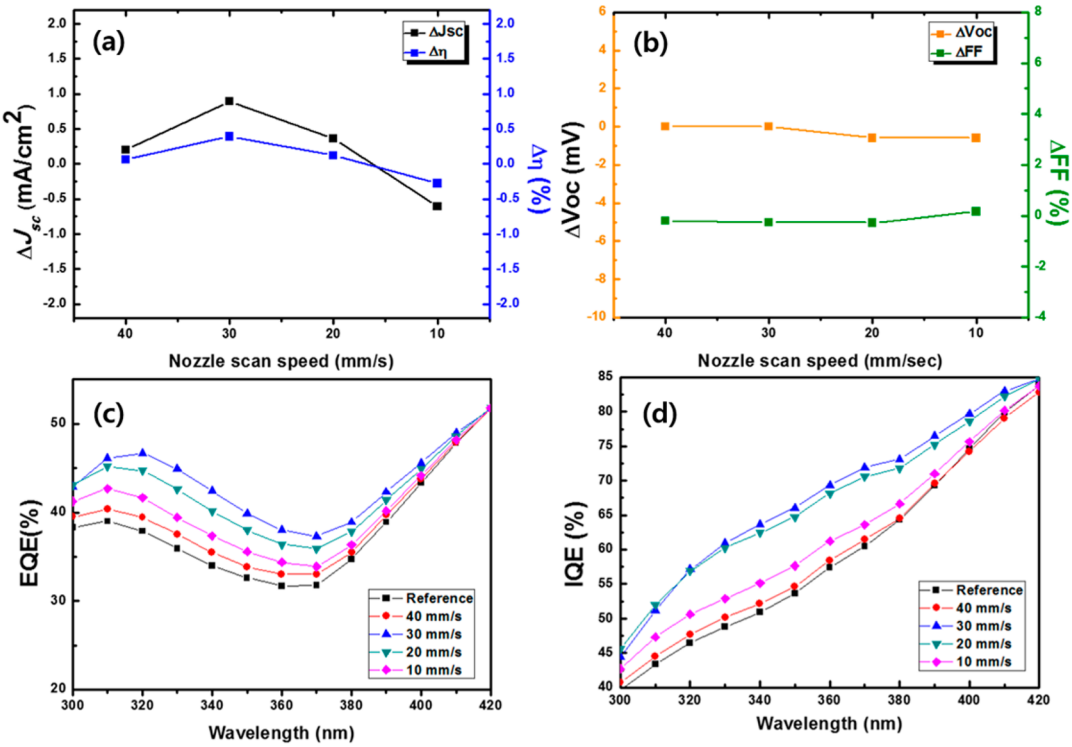

Figure 6. Performance parameters of solar cells with down-shift layers: (a) changes in short-circuit current density, ΔJ_{sc}, and efficiency, $\Delta\eta$; (b) changes in open-circuit voltage, ΔV_{oc}, and fill factor, ΔFF; (c) external quantum efficiency, EQE; and (d) internal quantum efficiency, IQE.

DOI: 10.1021/acsami.5b03672
ACS Appl. Mater. Interfaces 2015, 7, 19043−19049

efficiency (EQE), internal quantum efficiency (IQE), and light $I-V$ data analysis. (PDF)

AUTHOR INFORMATION

Corresponding Authors

*E-mail: solar@korea.ac.kr.
*E-mail: lhseok@korea.ac.kr.
*E-mail: ddang@korea.ac.kr.

Author Contributions

The manuscript was written through contributions of all authors. All authors have given approval to the final version of the manuscript.

Notes

The authors declare no competing financial interest.

ACKNOWLEDGMENTS

This work was supported by the Human Resources Development Program (No. 20124030200120) and by the New & Renewable Energy Core Technology Program (No. 20133010011780) of the Korea Institute of Energy, Technology, Evaluation and Planning (KETEP) under the auspices of the Ministry of Trade, Industry and Energy, Republic of Korea.

ABBREVIATIONS

AFM	atomic force microscopy
GO	graphene oxide
GQDs	graphene quantum dots
HRSEM	high-resolution scanning electron microscopy
PL	photoluminescence
TEM	transmission electron microscopy
EDS	energy-dispersive spectroscopy
XPS	X-ray photoelectron spectroscopy

REFERENCES

(1) Seidel, H.; Csepregi, L.; Heuberger, A.; Baumgartel, H. Anisotropic Etching of Crystalline Silicon in Alkaline Solutions. *J. Electrochem. Soc.* **1990**, *137*, 3612−3626.

(2) Papet, P.; Nichiporuk, O.; Kaminski, A.; Rozier, Y.; Kraiem, J.; Lelievre, J.-F.; Chaumartin, A.; Fave, A.; Lemiti, M. Pyramidal Texturing of Silicon Solar Cell with TMAH Chemical Anisotropic Etching. *Sol. Energy Mater. Sol. Cells* **2006**, *90*, 2319−2328.

(3) Kim, J.; Inns, D.; Fogel, K.; Sadana, D. K. Surface Texturing of Single-Crystalline Silicon Solar Cells Using Low Density SiO_2 Films as an Anisotropic Etch Mask. *Sol. Energy Mater. Sol. Cells* **2010**, *94*, 2091−2093.

(4) Li, J.; Lu, Y.; Lan, P.; Zhang, X.; Xu, W.; Tan, R.; Song, W.; Choy, K.-L. Design, Preparation, and Durability of TiO_2/SiO_2 and ZrO_2/SiO_2 Double-Layer Antireflective Coatings in Crystalline Silicon Solar Modules. *Sol. Energy* **2013**, *89*, 134−142.

(5) Lelievre, J.-F.; Fourmond, E.; Kaminski, A.; Palais, O.; Ballutaud, D.; Lemiti, M. Study of the Composition of Hydrogenated Silicon Nitride SiN_x:H for Efficient Surface and Bulk Passivation of Silicon. *Sol. Energy Mater. Sol. Cells* **2009**, *93*, 1281−1289.

(6) Hameiri, Z.; Mai, L.; Puzzer, T.; Wenham, S. R. Influence of Laser Power on the Properties of Laser Doped Solar Cells. *Sol. Energy Mater. Sol. Cells* **2011**, *95*, 1085−1094.

(7) Ferrada, P.; Harney, R.; Wefringhaus, E.; Lossen, J.; Meyer, K. Diffusion through Semitransparent Barriers on P-Type Silicon Wafers. In *Proceedings of the 24th European Photovoltaic Solar Energy Conference*, Hamburg, Germany, 2009, 1897−1900.

(8) Schubert, G.; Huster, F.; Fath, P. Current Transport Mechanism in Printed Ag Thick Film Contacts to an N-Type Emitter of a Crystalline Silicon Solar Cell. In *Proceedings of the 19th European Photovoltaic Solar Energy Conference*, Paris, France, 2004, 813−816.

(9) Park, S.; Song, J.; Tark, S. J.; Kim, Y. D.; Choi, C.; Kwon, S.; Yoon, S.; Son, C.-S.; Kim, D. Investigation of Al Back Contacts and BSF Formation by In Situ TEM for Silicon Solar Cells. *Prog. Photovoltaics* **2014**, *22*, 863−869.

(10) Horteis, M.; Glunz, S. W. Fine Line Printed Silicon Solar Cells Exceeding 20% Efficiency. *Prog. Photovoltaics* **2008**, *16*, 555−560.

(11) Kerschaver, E. V.; Beaucarne. Back-Contact Solar Cells: A Review. G. *Prog. Photovoltaics* **2006**, *14*, 107−123.

(12) Franklin, E.; Fong, K.; McIntosh, K.; Fell, A.; Blakers, A.; Kho, T.; Walter, D.; Wang, D.; Zin, N.; Stocks, M.; Wang. E.; Grant, N.; Wan, Y.; Yang, Y.; Zhang, X.; Verlinden, P. J. Design, Fabrication and Characterization of a 24.4% Efficient Interdigitated Back Contact Solar Cell. In *Proceedings of the 29th European Photovoltaic Solar Energy Conference*, Amsterdam, The Netherlands, 2014, 666-671.

(13) Zhao, J.; Wang, A.; Green, M. A. 24.5% Efficiency Silicon PERT Cells on MCZ Substrates and 24.7% Efficiency PERL Cells on FZ Substrates. *Prog. Photovoltaics* **1999**, *7*, 471−474.

(14) Sawada, T.; Terada, N.; Tsuge, S.; Baba, T.; Takahama, T.; Wakisaka, K.; Tsuda, S.; Nakano, S. High-Efficiency a-Si/c-Si Heterojunction Solar Cell. In *Proceedings of IEEE WCPEC*, Hawaii, 1994, 1219−1226.

(15) Taguchi, M.; Yano, A.; Tohoda, S.; Matsuyama, K.; Nishiwaki, T.; Fujita, K.; Maruyama, E. 24.7% Record Efficiency HIT Solar Cell on Thin Silicon Wafer. *IEEE J. Photovoltaics* **2014**, *4*, 96−99.

(16) Atwater, H. A.; Polman, A. Plasmonics for Improved Photovoltaic Devices. *Nat. Mater.* **2010**, *9*, 205−213.

(17) Zhang, Y.; Ouyang, Z.; Stokes, N.; Jia, B.; Shi, Z.; Gu, M. Low Cost and High Performance Al Nanoparticles for Broadband Light Trapping in Si Wafer Solar Cells. *Appl. Phys. Lett.* **2012**, *100*, 151101−1−4.

(18) Fosli, C. H.; Thogersen, A.; Karazhanov, S.; Marstein, E. S. Plasmonics for Light Trapping in Silicon Solar Cells. *Energy Procedia* **2011**, *10*, 287−291.

(19) Fahim, N. F.; Ouyang, Z.; Jia, B.; Zhang, Y.; Shi, Z.; Gu, Z. Enhanced Photocurrent in Crystalline Silicon Solar Cells by Hybrid Plasmonic Antireflection Coatings. *Appl. Phys. Lett.* **2012**, *101*, 261102−1−5.

(20) Zhang, Y.; Stokes, N.; Jia, B.; Fan, S.; Gu, M. Towards Ultra-Thin Plasmonic Silicon Wafer Solar Cells with Minimized Efficiency Loss. *Sci. Rep.* **2014**, *4*, 1−6.

(21) Hagglund, C.; Zach, M.; Kasemo, B. Enhanced Charge Carrier Generation in Dye Sensitized Solar Cells by Nanoparticle Plasmons. *Appl. Phys. Lett.* **2008**, *92*, 013113−1−5.

(22) Chen, X.; Jia, B.; Saha, J. K.; Cai, B.; Stokes, N.; Qiao, Q.; Wang, Y.; Shi, Z.; Gu, M. Broadband Enhancement in Thin-film Amorphous Silicon Solar Cells Enabled by Nucleated Silver Nanoparticles. *Nano Lett.* **2012**, *12*, 2187−2192.

(23) Tan, H.; Santbergen, R.; Smets, A. H. M.; Zeman, M. Plasmonic Light Trapping in Thin-film Silicon Solar Cells with Improved Self-Assembled Silver Nanoparticles. *Nano Lett.* **2012**, *12*, 4070−4076.

(24) Dong, Y.; Li, G.; Zhou, N.; Wang, R.; Chi, Y.; Chen, G. Graphene Quantum Dot as a Green and Facile Sensor for Free Chlorine in Drinking Water. *Anal. Chem.* **2012**, *84*, 8378−8382.

(25) Jiang, F.; Chen, D.; Li, R.; Wang, Y.; Zhang, G.; Li, S.; Zheng, J.; Huang, N.; Gu, Y.; Wang, C.; Shu, C. Eco-Friendly Synthesis of Size-Controllable Amine-Functionalized Graphene Quantum Dots with Antimycoplasma Properties. *Nanoscale* **2013**, *5*, 1137−1142.

(26) Son, Y.-W.; Cohen, M. L.; Louie, S. G. Energy Gaps in Graphene Nanoribbons. *Phys. Rev. Lett.* **2006**, *97*, 216803.

(27) Nakada, K.; Fujita, M.; Dresselhaus, G.; Dresselhaus, M. S. Edge State in Graphene Ribbons: Nanometer Size Effect and Edge Shape Dependence. *Phys. Rev. B: Condens. Matter Mater. Phys.* **1997**, *54*, 17954−17961.

(28) Shen, J.; Zhu, Y.; Yang, X.; Zong, J.; Zhang, J.; Li, C. One-Pot Hydrothermal Synthesis of Graphene Quantum Dots Surface-Passivated by Polyethylene Glycol and Their Photoelectric conversion under near-infrared light. *New J. Chem.* **2012**, *36*, 97−101.

(29) Li, Y.; Zhao, Y.; Shi, G.; Deng, L.; Hou, Y.; Qu, L. An Electrochemical Avenue to Green-Luminescent Graphene Quantum

DOI: 10.1021/acsami.5b03672
ACS Appl. Mater. Interfaces 2015, 7, 19043−19049

Dots as Potential Electron-Acceptors for Photovoltaics. *Adv. Mater.* **2011**, *23*, 776−780.
(30) Gupta, V.; Chaudhary, N.; Srivastava, R.; Sharma, G. D.; Bhardwaj, R.; Chand, S. Luminscent Graphene Quantum Dots for Organic Photovoltaic Devices. *J. Am. Chem. Soc.* **2011**, *133*, 9960−9963.
(31) Ran, X.; Sun, H.; Pu, F.; Ren, J.; Qu, X. Ag Nanoparticle-Decorated Graphene Quantum Dots for Label-Free, Rapid and Sensitive Detection of Ag^+ and Biothiols. *Chem. Commun.* **2013**, *49*, 1079−1081.
(32) Shen, J.; Zhu, Y.; Yang, X.; Li, C. Graphene Quantum Dots: Emergent Nanolights for Bioimaging, Sensors, Catalysis and Photovoltaic Devices. *Chem. Commun.* **2012**, *48*, 3686−3699.
(33) Kim, D.-Y.; Sinha-Ray, S.; Park, J.-J.; Lee, J.-G.; Cha, Y.-H.; Bae, S.-H.; Ahn, J.-H.; Jung, Y. C.; Kim, S. M.; Yarin, A. L.; Yoon, S. S. Self-Healing Reduced Graphene Oxide Films by Supersonic Kinetic Spraying. *Adv. Funct. Mater.* **2014**, *24*, 4986−4995.
(34) Hirata, M.; Gotou, T.; Horiuchi, S.; Fujiwara, M.; Ohba, M. Thin-film Particles of Graphite Oxide 1: High-Yield Synthesis and Flexibility of the Particles. *Carbon* **2004**, *42*, 2929−2937.
(35) Pei, S.; Cheng, H.-M. The Reduction of Graphene Oxide. *Carbon* **2012**, *50*, 3210−3228.
(36) Berger, C.; Song, Z.; Li, X.; Wu, X.; Brown, N.; Naud, C.; Mayou, D.; Li, T.; Hass, J.; Marchenkov, A. N.; Conrad, E. H.; First, P. N.; Heer, W. A. Electronic Confinement and Coherence in Patterned Epitaxial Graphene. *Science* **2006**, *312*, 1191−1196.
(37) Ko, Y. U.; Cho, S.; Choi, K. S.; Park, Y.; Kim, S. T.; Kim, N. H.; Kim, S. Y.; Chang, S. T. Microlitre Scale Solution Processing for Controlled, Rapid Fabrication of Chemically Derived Graphene Thin Films. *J. Mater. Chem.* **2012**, *22*, 3606−3613.
(38) Lee, K. D.; Dahiwale, S. S.; Kim, Y. D.; Lee, J.-H.; Kim, S.; Bae, S.; Park, S.; Tark, S. J.; Kim, D. Influence of SiN_x:H Films Properties According to Gas Mixture Ratios for Crystalline Silicon Solar Cells. *Curr. Appl. Phys.* **2013**, *13*, 241−245.
(39) Irissou, E.; Legoux, J.-G.; Ryabinin, A. N.; Jodoin, B.; Moreau, C. Review on Cold Spray Process and Technology: Part1-Intellectual Property. *J. Therm. Spray Technol.* **2008**, *17*, 495−516.
(40) Kim, J. K.; Park, M. J.; Kim, S. J.; Wang, D. H.; Cho, S. P.; Bae, S.; Park, J. H.; Hong, B. H. Balancing Light Absorptivity and Carrier Conductivity of Graphene Quantum Dots for High-Efficiency Bulk Heterojunction Solar Cells. *ACS Nano* **2013**, *7*, 7207−7212.
(41) Minati, L.; Torrengo, S.; Maniglio, D.; Migliaresi, C.; Speranza, G. Luminescent Graphene Quantum Dots from Oxidized Multi-Walled Carbon Nanotubes. *Mater. Chem. Phys.* **2012**, *137*, 12−16.
(42) Waters, M. L. Aromatic Interactions in Model Systems. *Curr. Opin. Chem. Biol.* **2002**, *6*, 736−741.
(43) Sindkhedkar, M. D.; Mulla, H. R.; Cammers-Goodwin, A. Three-State, Conformational Probe for Hydrophobic, π-stacking Interactions in Aqueous and Mixed Aqueous Solvent Systems: Anisotropic Solvation of Aromatic Rings. *J. Am. Chem. Soc.* **2000**, *122*, 9271−9277.
(44) Zhou, Y.; Bao, Q.; Tang, L. A. L.; Zhong, Y.; Loh, K. P. Hydrothermal Dehydration for the "Green" Reduction of Exfoliated Graphene Oxide to Graphene and Demonstration of Tunable Optical Limiting Properties. *Chem. Mater.* **2009**, *21*, 2950−2956.
(45) Ferrari, A. C.; Meyer, J. C.; Scardaci, V.; Casiraghi, C.; Lazzeri, M.; Mauri, F.; Piscanec, S.; Jiang, D.; Novoselov, K. S.; Roth, S.; Geim, A. K. Raman Spectrum of Graphene and Graphene Layers. *Phys. Rev. Lett.* **2006**, *97*, 187401.

DOI: 10.1021/acsami.5b03672
ACS Appl. Mater. Interfaces 2015, 7, 19043−19049